

# On the Cycling Performance of Na-O<sub>2</sub> Cells: Revealing the Impact of the Superoxide Crossover toward the Metallic Na Electrode

Xiaoting Lin, Qian Sun, Hossein Yadegari, Xiaofei Yang, Yang Zhao, Changhong Wang, Jianneng Liang, Alicia Koo, Ruying Li, and Xueliang Sun\*

Na-O<sub>2</sub> batteries have attracted extensive attention as promising candidates for large-scale energy storage due to their ultrahigh theoretical energy density. However, the poor cycling performance of Na-O<sub>2</sub> batteries is one of the major challenges facing its future development. A novel Na-O<sub>2</sub> battery using electrically connected carbon paper with Na metal as a protected anode is presented in this study. The O<sub>2</sub><sup>-</sup> crossover from the cathode to anode partially contributes to the limited Coulombic efficiency, as well as the Na corrosion during the cycling process. For the cells with protected Na, the carbon paper maintains a pseudo-equal potential with the Na metal and works as an artificial protective layer to suppress the detrimental side reactions caused by O<sub>2</sub><sup>-</sup> and O<sub>2</sub> crossover toward the Na electrode. Furthermore, the short-circuiting issue caused by Na dendrite growth also can be completely resolved. Consequently, the Na-O<sub>2</sub> cells with protected Na exhibit two times higher discharge capacity and cycling stability compared with the cells using bare Na. These results indicate the crucial role of the Na anode in determining the overall cell performance and a rational design of anode can dramatically contribute to develop advanced Na-O<sub>2</sub> batteries with longer lifespans and better cycling performance.

metal-oxygen batteries.<sup>[2]</sup> Despite the fact that the rechargeable Li-O<sub>2</sub> batteries deliver a much higher energy density compared to other metal-oxygen battery systems, future development of Li-O<sub>2</sub> batteries have been hindered by scientific challenges, especially the high charge overpotential.<sup>[3]</sup> As an alternative of Li-O<sub>2</sub> battery, superoxide Na-O<sub>2</sub> batteries are more promising for future applications in terms of good reversibility, high round-trip energy efficiency, and clean chemistry.<sup>[4]</sup> However, the poor cycling performance is still one of the major challenges faced by state-of-the-art Na-O<sub>2</sub> batteries, and this critical problem will need to be properly addressed before it can be used in practical applications.

It is well accepted that the characteristics of the air electrodes, such as pore volume, pore size distribution, and surface area are key to achieving high-performance Na-O<sub>2</sub> batteries.<sup>[5]</sup> Meanwhile, the presence of aprotic additives, the selection of organic

electrolyte, conducting salts, binder, and even humidity have a profound effect on the Na-O<sub>2</sub> (or Na-air) cell performance.<sup>[6]</sup> In this regard, much effort has been devoted to investigating the underlying mechanisms at the air electrode side of Na-O<sub>2</sub> batteries. In contrast, as another key component of Na-O<sub>2</sub> batteries, the effect of metallic Na anode on the cell performance has been seldom studied in detail.<sup>[7]</sup> Up to now, there have been a number of papers showing that Na-O<sub>2</sub> batteries with metallic Na anode may suffer from a short-circuiting issue induced by Na dendrite growth, leading to premature cell death and safety concerns. Nonetheless, it is still widely presumed that the air electrode (cathode) plays the most important role in the electrochemical performance of Na-O<sub>2</sub> batteries. Therefore, very few research in the field of Na-O<sub>2</sub> battery have focused on the anode side.


The observation of Na dendrite growth in Na-O<sub>2</sub> battery was first reported by Guo and co-workers.<sup>[7a]</sup> The origin of Na dendrite growth in Na-O<sub>2</sub> battery system has also been reported and studied by Janek and co-workers, where a ceramic Na<sup>+</sup> conductor was used to suppress the dendrite growth in their reports.<sup>[7c,8]</sup> In another study, they replaced the Na metal anode with a sodiated carbon anode, achieving improved cycling

## 1. Introduction

Metal-oxygen batteries have recently attracted an extensive amount of attention as one of the most promising power sources for next generation electric vehicles and large-scale stationary electricity storage due to their ultrahigh theoretical energy densities.<sup>[1]</sup> In the past few decades, remarkable scientific advances have been made in elucidating the electrochemistry of various

X. Lin, Dr. Q. Sun, Dr. H. Yadegari, X. Yang, Y. Zhao, C. Wang, J. Liang, A. Koo, R. Li, Prof. X. Sun  
Department of Mechanical and Materials Engineering  
University of Western Ontario  
London, Ontario N6A 5B9, Canada  
E-mail: xsun@eng.uwo.ca

X. Yang  
Division of Energy Storage  
Dalian Institute of Chemical Physics  
Chinese Academy of Science  
Zhongshan Road 457, Dalian 116023, China

 The ORCID identification number(s) for the author(s) of this article can be found under <https://doi.org/10.1002/adfm.201801904>.

DOI: 10.1002/adfm.201801904

life and energy efficiency.<sup>[9]</sup> Nonetheless, from a practical perspective, the low capacity of current carbon anode for sodium batteries may still be insufficient to match the large capacity of air electrode. The importance of addressing challenges with regards to the anode were further confirmed with the application of sodium ion selective membranes in the research of Bi et al.<sup>[7b]</sup> However, this study on the understanding of the negative electrode in metal-O<sub>2</sub> batteries is still relatively scarce.

Compared with Li-O<sub>2</sub> cells, the dissolved Na<sup>+</sup>-O<sub>2</sub><sup>-</sup> in the Na-O<sub>2</sub> cells is more stable than its Li counterpart,<sup>[10]</sup> and a solution-based mechanism for the formation of NaO<sub>2</sub> have been widely reported.<sup>[5d,11]</sup> Therefore, the crossing over of O<sub>2</sub><sup>-</sup> toward negative electrode may be expected to be more severe in Na-O<sub>2</sub> cells. Previous studies have shown that the crossing over of O<sub>2</sub> from cathode can lead to ether-based electrolyte decomposition on the anode, which leads to serious side reactions on the anode.<sup>[4c,12]</sup> Undoubtedly, accumulation of contaminants on the Na surface results in suppressed Na<sup>+</sup> transportation and thus restricts the battery performance by imposing large charge/mass transfer overpotential during discharge and charge reactions. However, to the best of our knowledge, the crossing over of O<sub>2</sub><sup>-</sup> is rarely studied and its effect on Na-O<sub>2</sub> batteries is yet poorly understood.

In this paper, an electrically connected carbon paper (CP) and Na metal is fabricated and used as the protected Na anode in Na-O<sub>2</sub> batteries (Figure S1, Supporting Information). Interestingly, the adoption of this protected Na can dramatically improve the electrochemical performance and increase the cycling life of Na-O<sub>2</sub> batteries by shielding O<sub>2</sub><sup>-</sup> and O<sub>2</sub> crossover to suppress the detrimental side reactions on the Na anode surface. Moreover, the resultant configuration shows promising results for solving the short-circuiting issue by decreasing the local current density imposed to the anode. The presented results in this study indicate that the negative Na electrode in Na-O<sub>2</sub> cells greatly affects the overall performance of the battery and thus should be attracting further research attention in the future studies.

## 2. Results and Discussion

### 2.1. Electrochemical Behavior of Na-O<sub>2</sub> Cells with Bare Na and Protected Na Anode

In our previous studies, we have already shown that the electrochemical behavior and discharge products can be highly dependent on the configuration of the Na-O<sub>2</sub> battery and the choice of the air electrode materials.<sup>[5d,6a,13]</sup> In this study, we have chosen a commercial CP (H2315) as the air electrode, which has been widely used in different groups and the corresponding discharge product has been reported to be sodium superoxide (NaO<sub>2</sub>).<sup>[4b,6c,14]</sup> In order to examine the critical role of anode on the cell performance, the electrochemical discharge and charge cycles of Na-O<sub>2</sub> cells with and without protected Na were investigated at different areal current densities (Figure 1).

It can be clearly observed that the initial discharge capacities of the Na-O<sub>2</sub> cells increase significantly after introducing a CP onto the Na electrode (Figure 1a,b). Initial discharge capacities

of 5.52, 5.08, 3.56, and 1.66 mAh cm<sup>-2</sup> are achieved in the case of the cells with protected Na at current densities of 0.1, 0.2, 0.5, and 1.0 mA cm<sup>-2</sup>, respectively. In comparison, only less than 50% of the initial discharge capacities are delivered for the cells with bare Na at the same current densities (Figure S2a, Supporting Information). Moreover, it can be found that cells with bare Na exhibit the discharge plateau at around 2.0 V, which is slightly lower than that of the cells with protected Na at all current densities (Figure S2b, Supporting Information). To rule out any other possible beneficial contribution other than from the use of protected Na, all the other components of the cells including the air electrode and the cell electrolyte are kept the same. Therefore, it is evident that the significant increase of the initial discharge capacity can be solely related to the protected Na anode.

The discharge products generated during the discharge process was revealed by X-ray diffraction (XRD) for both cells, at the current density of 0.1 mA cm<sup>-2</sup> (Figure 2a,b). The diffraction peak positions of both discharged cathodes are consistent with that of NaO<sub>2</sub>, and no other side products can be observed. Meanwhile, it should be noted that the intensity of the NaO<sub>2</sub> peak on cathode obtained from the cell with protected Na is much stronger compared to the cell with bare Na (Figure S3, Supporting Information), indicating a larger amount of NaO<sub>2</sub> is produced in the cell with protected Na. This result agrees well with the larger discharge capacities of cell with protected Na compared with that of the cell with bare Na at the same current density of 0.1 mA cm<sup>-2</sup>. The formation of NaO<sub>2</sub> on the discharged cathode was further confirmed by the Raman signal at 1156 cm<sup>-1</sup> (Figure S4, Supporting Information), consistent with the previous report by Hartmann et al.<sup>[4b]</sup> Note that no Raman peaks of NaOH, Na<sub>2</sub>CO<sub>3</sub>, or other side products can be observed from the discharged air electrode in the cell with protected Na. Those results indicate that the application of CP on metallic Na anode does not change the nature of the discharge product, and NaO<sub>2</sub> is identified as the only discharge product in Na-O<sub>2</sub> battery with protected Na. In addition, the discharged air electrodes in the cells with and without protected Na were also investigated using scanning electron microscope (SEM), as shown in Figure 2c–f. Cubic shaped particles almost completely fill the pores on the oxygen side of the air electrode for the cell with protected Na. This contrasts with the cell assembled with bare Na where the electrochemical reaction terminates before the pores on the oxygen side of cathode become blocked or active electrode surface becomes completely covered.

According to previous reports, the precipitation of insoluble discharge products within the pores of the cathode may prevent the continuous O<sub>2</sub> transportation into the interior of the cathode.<sup>[15]</sup> Thus, it is not possible for the pores on the separator side of the air electrode to be fully covered when the oxygen diffusion channels on the oxygen side have already been blocked. A similar phenomenon was observed on both sides of the air electrode in the case of the cell with protected Na (Figure 2d,f), indicating that the ending of discharge for this cell is most likely due to the blocking of further oxygen diffusion caused by discharge product accumulation. However, it is very interesting to find that the discharge process of the Na-O<sub>2</sub> battery with bare Na terminates before the cathode is fully blocked by discharge products (Figure 2c,e). Those results suggest an underlying

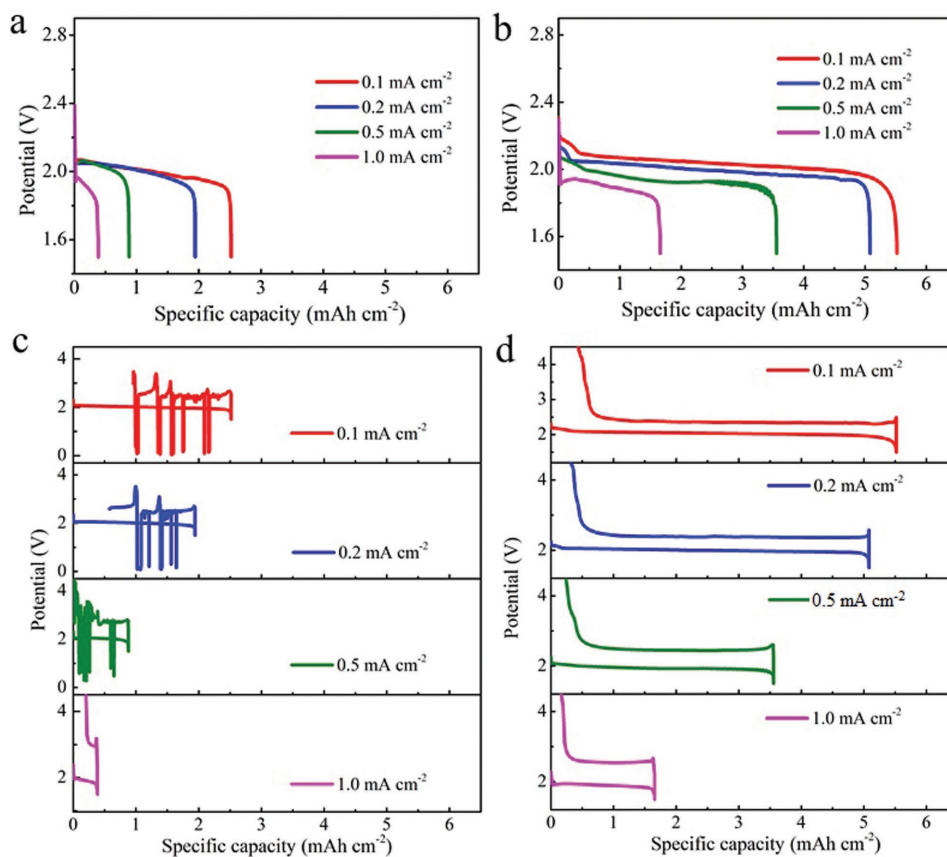


**Figure 1.** The initial discharge profiles of Na-O<sub>2</sub> cells with a) bare Na anode and b) protected Na anode at different current densities. The initial discharge/charge profiles of Na-O<sub>2</sub> cells with c) bare Na anode and d) protected Na anode in the potential range of 1.5–4.5 V versus Na/Na<sup>+</sup> at different current densities.

protective effect of the CP when electrically connected with Na metal during the discharge process, and the puzzle of this protective effect will be discussed in Section 2.3 of this study.

Aside from the distinct initial discharge capacity, the charging behavior of Na-O<sub>2</sub> cells with bare Na and protected Na anode are also notably different, regardless of the formation of the same discharge product in both cells. The potential of the cell with bare Na suddenly and repeatedly drops to almost 0 V after a charge capacity of  $\approx 0.35$  mAh cm<sup>-2</sup>, at a low current density of 0.1 mA cm<sup>-2</sup> (Figure 1c). This phenomenon is typical for the short-circuiting of the battery due to the growth and penetration of Na dendrites, which has also been observed in previous studies on Na-O<sub>2</sub> batteries.<sup>[7b,c]</sup> The recovery of the battery voltage is assumed to be the “melting and breaking down” of Na dendrite reaching the air electrode, shortly resolving the short-circuit until another dendrite reaches the air electrode. As a result, the discharge product of the Na-O<sub>2</sub> cell with bare Na will not be thoroughly decomposed (Figure S5a, Supporting Information). In addition, the short-circuiting of the cells is more severe at higher current densities of 0.2 and 0.5 mA cm<sup>-2</sup> as the first voltage drop occurs at lower charge capacities, which is caused by the accelerated Na dendrite growth at higher rates.<sup>[16]</sup> In contrast, the short-circuiting issue was completely addressed in the cells with protected Na, which showed a very smooth plateau at  $\approx 2.33$  V during the charge process. This value is very

close to the theoretical value (2.27 V) for the electrochemical decomposition of NaO<sub>2</sub> to form Na<sup>+</sup>, O<sub>2</sub> and an electron. Good reversibility of the Na-O<sub>2</sub> cells was further confirmed by XRD spectroscopy as the diffraction peaks of NaO<sub>2</sub> completely disappeared without forming any additional peaks after recharging (Figure S5b, Supporting Information). Moreover, it is necessary to emphasize that the Na-O<sub>2</sub> cells with protected Na displayed Coulombic efficiencies of more than 90%, even at a high current density of 1.0 mA cm<sup>-2</sup>. To the best of our knowledge, these results show some of the best cell performances using the same air electrode compared to other studies using similar current densities.<sup>[4b,6c,17]</sup>

## 2.2. The Direct Evidence on the Suppressing Effect of Protected Na on Dendrite Growth

To observe direct evidence that the Na-O<sub>2</sub> batteries short-circuited due to Na dendrite growth and penetration, we have disassembled the recharged cells for optical and SEM observations. As shown in Figure S6a–c (Supporting Information), a large number of dendritic spots can be observed on the bulk Na surface after the cell with bare Na anode short-circuited during the charging process ( $\approx 0.35$  mAh cm<sup>-2</sup>). In addition, the layered structure of a pristine separator is no longer observed

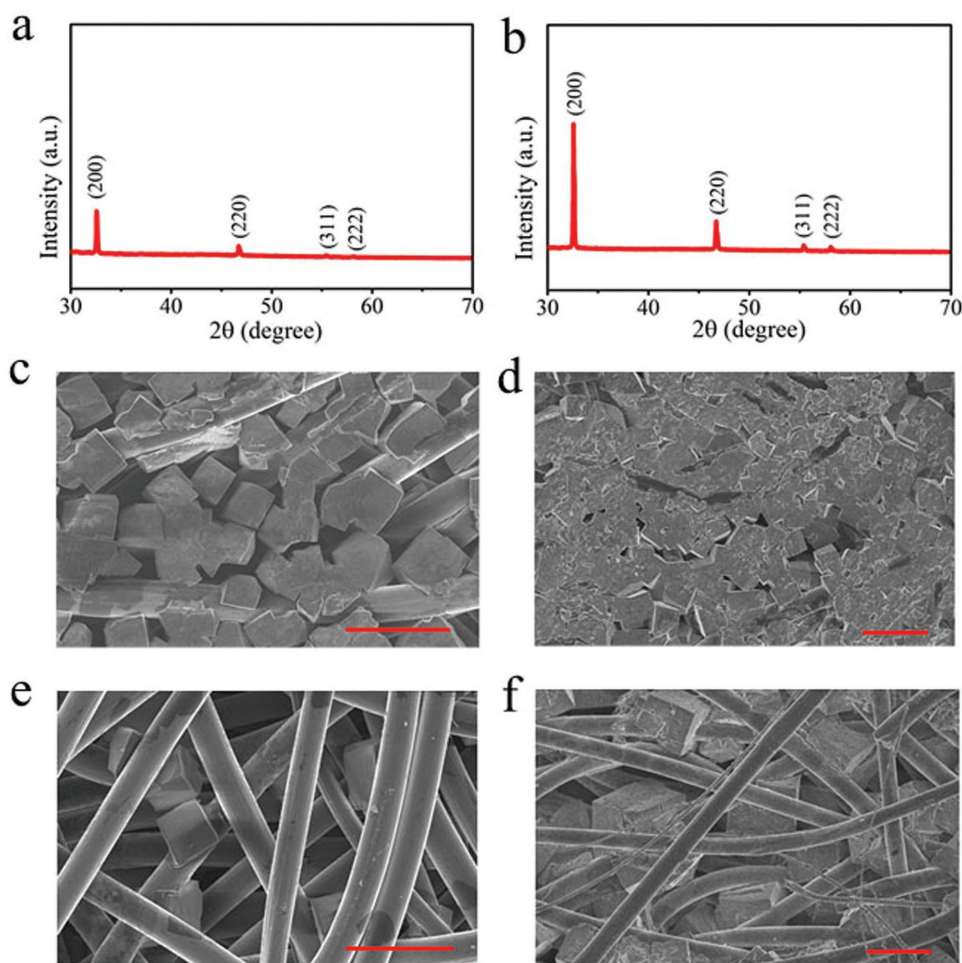


**Figure 2.** The a,b) XRD patterns and c–f) SEM images of fully discharged air electrodes in Na-O<sub>2</sub> cells with bare Na and protected Na anode at 0.1 mA cm<sup>-2</sup>; c,d) oxygen side and e,f) separator side of discharged air electrodes (scale bars = 20 μm).

due to the growth of Na dendrites filling the porous structure of the glass fiber (GF), leading to a stacked structure without obvious interlayer spacing according to the cross-sectional SEM images (Figures S6d–f and S7, Supporting Information). These results are consistent with several previous studies on the effect of Na dendrite on Na-O<sub>2</sub> batteries.<sup>[7]</sup> In contrast, the separator in the Na-O<sub>2</sub> cell with protected Na maintained its clean surface and clear layered structure after the cell was fully recharged at 0.1 mA cm<sup>-2</sup>, as no obvious Na deposits can be observed on the separator (Figure S8a,b, Supporting Information). Furthermore, both sides of CP extracted from the anode side of a charged cell was also examined by optical and SEM imaging. As shown in Figure S8c–f (Supporting Information), different morphologies were found on the two sides of the CP after the cell was fully recharged (≈5.0 mAh cm<sup>-2</sup>). The metal luster morphology of the bulk Na side of the CP indicates that a large amount of Na deposit is confined inside the matrix, while no obvious Na deposits can be seen on the separator side.

To further clarify the deposition behavior of Na on the anode in the cell with a protected Na, the morphology of the CP at different electrochemical states was investigated by SEM (Figure 3a–d). Interestingly, different morphologies can be observed from cross-sectional SEM images of the two sides of

the CP that are connected to the separator and the Na electrode after the cell was fully discharged. As shown in Figure 3a, the surface of the CP facing the Na side seems cleaner than that facing the separator side. The latter is almost fully covered by amorphous film-like products. Further examining the surface of the CP by SEM (Figure S9a,b) also revealed a greater accumulation of deposits on the separator side of the CP. Raman testing was performed to identify the chemical nature of the deposits on the CP surface, where Na<sub>2</sub>CO<sub>3</sub> and NaOH were identified as the main phase of the side products, and no characteristic peak of NaO<sub>2</sub> was detected in the Raman spectrum from the CP surface (Figure S9c, Supporting Information). Noted that alkali metal is inherently unstable when in contact with organic electrolyte due to the low redox potential, leading to the formation of solid electrolyte interphase (SEI) on the alkali metal surface. CH<sub>3</sub>OLi, CH<sub>3</sub>Li, and polymeric layers are the main decomposition products of an ether-based electrolyte on Li surface in Li-ion batteries (LIBs).<sup>[18]</sup> While in Li-O<sub>2</sub> batteries, different electrolyte decomposition reactions can be observed compared with that in LIBs, and the formation of LiOH and carbonates on the Li anode is predominantly due to the oxygen crossover effect.<sup>[12a,19]</sup> Similar electrolyte decomposition mechanism has also been reported in K-O<sub>2</sub> batteries in the presence of O<sub>2</sub>



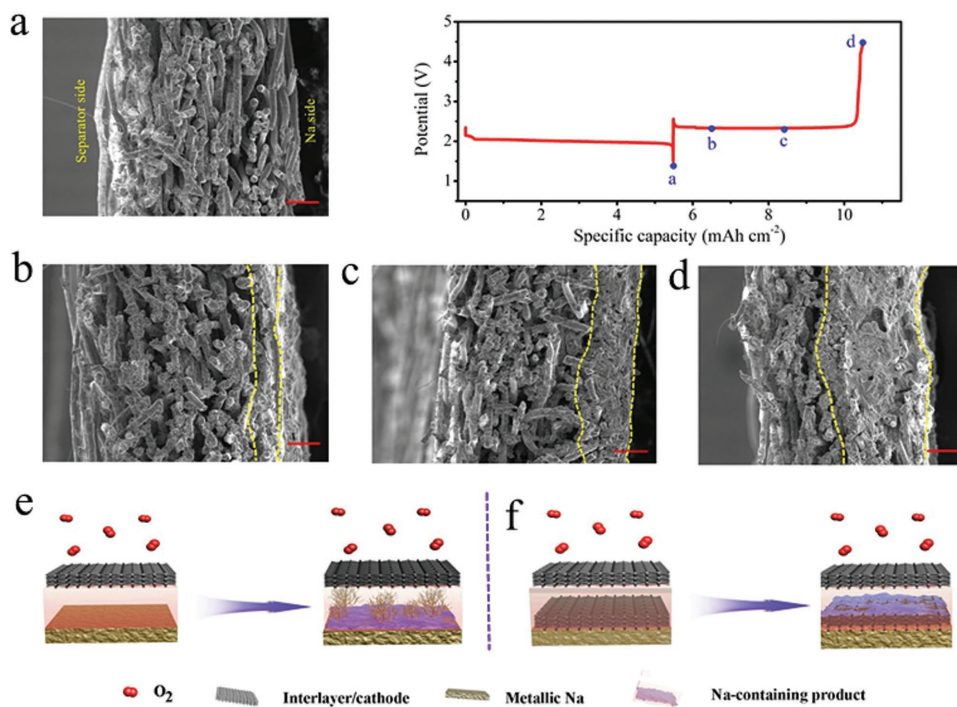


**Figure 3.** The cross-sectional SEM images of CP with different amount of Na deposits. a)  $0 \text{ mAh cm}^{-2}$ , b)  $1 \text{ mAh cm}^{-2}$ , c)  $3 \text{ mAh cm}^{-2}$ , and d)  $\approx 5 \text{ mAh cm}^{-2}$  (scale bars =  $50 \text{ }\mu\text{m}$ ), the distance between two dotted yellow line showing the thickness of deposited Na during charging process; schematic diagrams of sodium deposition in cells with e) bare Na and f) protected Na.

crossover.<sup>[4c]</sup> More side products were observed on the CP at the separator side compared to the Na side in our case, which is identical to the migration direction of  $\text{O}_2$  and  $\text{O}_2^-$  from the air electrode toward the Na electrode. Therefore, the  $\text{Na}_2\text{CO}_3$  and  $\text{NaOH}$  on the CP could be formed by the reaction between  $\text{O}_2^-$  with the electrolyte and the CP, and also the decomposition of the electrolyte in the presence of  $\text{O}_2$ .

In the subsequent charging process, as shown in Figure 3b, Na was preferentially nucleated on the bulk Na side of the CP rather than the other side when plating  $1 \text{ mAh cm}^{-2}$  of Na, as shown in the area outlined with two dotted yellow lines. This is perhaps caused by the initial nucleation of Na on the bulk Na surface due to the lower nucleation barrier, compared with that on the CP structure. On the other hand, the presence of nonconductive  $\text{Na}_2\text{CO}_3$  and  $\text{NaOH}$  on the separator side of the CP may also contribute to the preferential deposition of Na on the other side. Further increasing the Na deposition capacity to  $3 \text{ mAh cm}^{-2}$ , the voids on the Na side of the CP were gradually filled with deposited Na to a thickness of  $\approx 30 \text{ }\mu\text{m}$  (Figure 3c). When the cell with protected Na was fully charged with  $\approx 5 \text{ mAh cm}^{-2}$  of Na deposit, about half of the inner space in the CP was filled by deposited Na, as shown in Figure 3d. Then, the CP surface was further studied using Raman and SEM technique, and more products can be observed on the separator side of CP interlayer compared with that at discharge state. However, the composition of the deposits on the CP surface keeps the same,  $\text{NaOH}$  and  $\text{Na}_2\text{CO}_3$  are still identified as the main phases based on the Raman characterization (Figure S9d,e, Supporting Information), indicating the occurrence of same reactions on the CP during the discharge and charge process.

In the  $\text{Na-O}_2$  cell with protected Na, the presence of a CP on the Na metal facilitates dense Na deposition without dendritic Na growth and thus prevents the cell from short-circuiting. This could be related to the lower current density in the presence of a 3D conductive network during the Na plating process. Combining the electrochemical properties of the cells with different configurations, it can be concluded that the difference in charging behavior between the cells with and without protected Na can be related to the CP conductivity.

Recent studies have reported that  $\text{NaPF}_6$  is capable of forming a uniform and compact SEI on the Na electrode in diglyme, while the SEI formed using other electrolyte salts, including  $\text{NaSO}_3\text{CF}_3$ ,  $\text{NaN}(\text{SO}_2\text{CF}_3)_2$ , and  $\text{NaClO}_4$ , is less uniform and compact in nature.<sup>[6b,20]</sup> This causes more Na to be exposed to undesirable side reactions with electrolytes, and, at the same time, the rough surface of metallic Na would result in uneven charge distribution and subsequent dendrite growth during the charging process. The low shear modulus of SEI layer formed on the Na surface is easier to be puncture with Na dendrites, and the short-circuit will occur after the Na dendrites penetrate the separator. Schematic of Na deposition on the anode of cells with bare Na and protected Na anode are shown in Figure 3e,f.

### 2.3. Understanding the Superoxide Radical Crossover in $\text{Na-O}_2$ Batteries with Protected Na Anode

However, the mystery of why the  $\text{Na-O}_2$  battery with protected Na can also significantly increase its discharge capacity and

Coulombic efficiencies compared to that of the cells with bare Na remains. In order to rule out the possible impact from merely the Na dendrite growth, capacity-limited cycling of the Na-O<sub>2</sub> cells with bare Na and protected Na were further investigated. The cut-off capacity of the cells is 0.1 mAh cm<sup>-2</sup>, which is much lower than the above-mentioned initial short-circuit capacities (ISCCs) of the batteries and thus the effect of Na dendrite formation and growth can be minimized.

Long-term cycling stability of the Na-O<sub>2</sub> cells were investigated at a current density of 0.1 mA cm<sup>-2</sup>, with a fixed discharge capacity of 0.1 mAh cm<sup>-2</sup> (Figure 4). Interestingly, as shown in Figure 4a,b, a stable discharge plateau at ≈2.0 V only remains for 14 cycles in the case of Na-O<sub>2</sub> cell with bare Na. The cell then starts to fail to deliver the defined discharge capacity and the cell shows an accelerated degradation afterward. At the 20th cycle, the cell maintains only ≈20% of its initial capacity. In sharp contrast, the cell with protected Na can stably run for over 65 cycles with a high Coulombic efficiency of ≈90%, which is much higher than that (≈70%) of the cell with bare Na anode (Figure 4c,d). Although the Na-O<sub>2</sub> cell with protected Na exhibits an overpotential gap of 0.16 V in the initial cycle that increases gradually to 0.36 V in the 60th cycle, the decomposition potential of NaO<sub>2</sub> has been consistently much lower than that of the cell with bare Na anode. There is no doubt that the lower charge transfer resistance of the cell with protected Na partially contributes to the better electrochemical performance, compared with that of the cell with bare Na anode (Figure S10, Supporting Information). However, it should also be noted that the cell with bare Na exhibited a much higher charge overpotential after the first cycle. The obvious increase of charge overpotential can be related to the increased resistance of the Na electrode caused by an accumulation of side products. While

in the case of the cell with protected Na, a relatively slower increase in the charge overpotential can be observed, which may be attributed to the alleviation of side reactions on the Na surface. Those results clearly indicate that the CP at the anode side has played another protective role during the discharge process of Na-O<sub>2</sub> batteries.

To reveal the nature of this protective effect, two different Na-O<sub>2</sub> cell configurations with exactly the same sodium anode, electrolyte and air electrode were constructed. For the first cell, two layers of GF were used as the separator (Figure 5a). We designed another cell by placing the CP between two GF separators instead of onto the Na anode (Figure 5b). However, the electrochemical performance of the cell with a CP sandwiched between the two GF separators had no significant difference compared to the cell with only two GF separator, exhibiting both the short-circuit effect at very close ISCCs and a relatively low discharge capacity. These results indicate that the protective role of the CP is not simply originated from itself but a synergy effect when it is combined with Na anode.

We anticipate the answer to this puzzle can be related to the nature of the inner reaction mechanism of Na-O<sub>2</sub> batteries. Recent studies have shown that the discharge process of Na-O<sub>2</sub> batteries that produces superoxide mostly involves a solution-based route, where the first step is the formation of a dissolvable O<sub>2</sub><sup>-</sup> anion or HO<sub>2</sub> via an electrochemical reduction of O<sub>2</sub> gas, followed by a precipitation step to form NaO<sub>2</sub> as the final discharge product. To address the origin of the limited Coulombic efficiency in Na-O<sub>2</sub> cells, which is another limiting factor for the cycling performance of the battery, we examined the cell separator after the full discharge at 0.1 mA cm<sup>-2</sup>. It should be noted that cubic NaO<sub>2</sub> with the diameter of 10 μm can also be observed on the cell separator (Figure S11a,b,

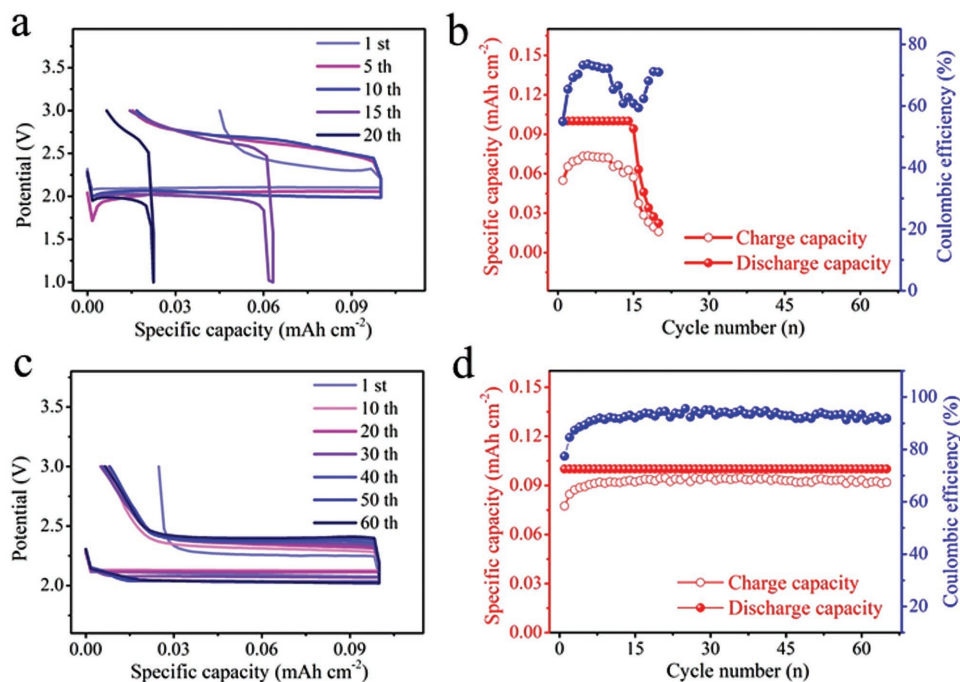


**Figure 4.** The selected charge/discharge curves of Na-O<sub>2</sub> cells with a) bare Na and c) protected Na anode. The cycling properties and Coulombic efficiency of Na-O<sub>2</sub> cells with b) bare Na and d) protected Na anode.

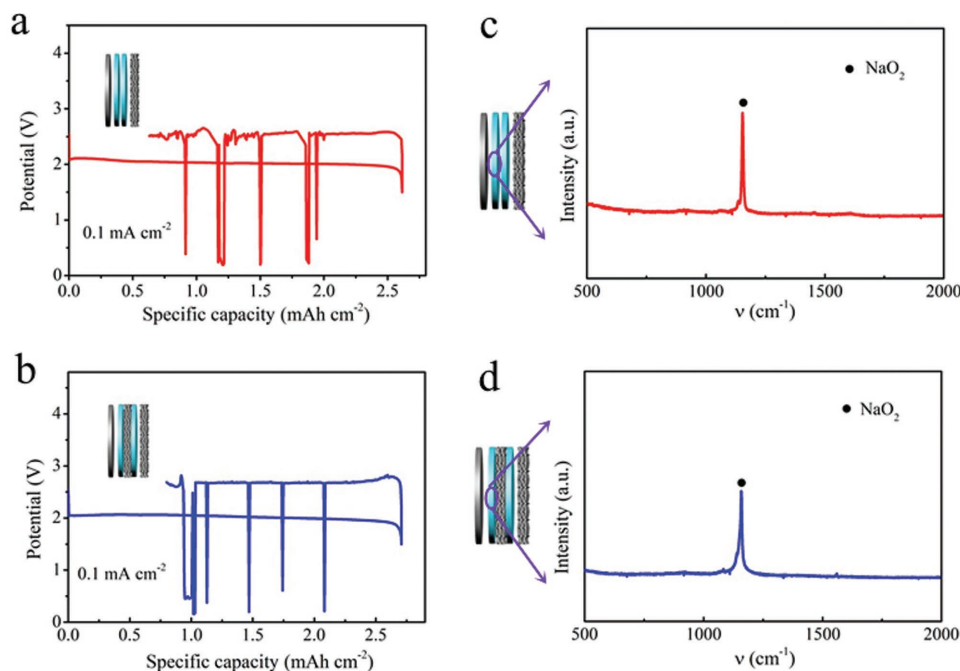


**Figure 5.** a,b) Schematic diagram of Na-O<sub>2</sub> cells with different separators and corresponding charge/discharge curve at a current density of 0.1 mA cm<sup>-2</sup>; c,d) Raman spectra of GF next to the Na anode after the cell fully discharged at 0.1 mA cm<sup>-2</sup>.

Supporting Information), which is indisputable evidence for the solution-mediated mechanism of NaO<sub>2</sub> formation. Similar observations with NaO<sub>2</sub> deposited on separators have also been reported by other groups.<sup>[11b]</sup> The O<sub>2</sub><sup>-</sup> produced during the discharge process dissolves into the electrolyte, and nucleation occurs once its concentration reaches the supersaturation threshold. It should be noted that the precipitated NaO<sub>2</sub> on the separator can also be detected by XRD (Figure S11c, Supporting Information), indicating that a considerable amount of O<sub>2</sub><sup>-</sup> can arrive at the separator and precipitate on its surface. Based on the presented evidence, it is reasonable to assume that a high concentration of O<sub>2</sub><sup>-</sup> exists around the separator. Moreover, it is reasonable to suspect that the O<sub>2</sub><sup>-</sup> radical likely migrates toward the Na anode due to the dual effect of an ion concentration gradient and electric field.

Na-O<sub>2</sub> cells with different separators were further constructed in order to examine the efficiency of the separator in blocking the migration of O<sub>2</sub><sup>-</sup> from the cathode to anode (Figure 5c,d). The thickness of the separator in both cells was increased compared to the cell with only one layer of GF (Figure 2a). However, examining the separator by Raman in two cell configurations indicates that the O<sub>2</sub><sup>-</sup> crossover also cannot be totally inhibited by increasing the thickness of separator, as the Raman signal of NaO<sub>2</sub> can still be detected on the second layer of GF (next to the Na electrode) after the cell fully discharged at 0.1 mA cm<sup>-2</sup>. As the low compact nature of SEI layer formed on the Na surface is insufficient to completely block the diffusion of O<sub>2</sub><sup>-</sup>, the chemical reduction of O<sub>2</sub><sup>-</sup> at the Na surface is therefore highly probable. Consequently, the migrated O<sub>2</sub><sup>-</sup> cannot be recovered during the charge cycle which in turn causes the limited Coulombic efficiency in Na-O<sub>2</sub> cells. This phenomenon is very similar to the well-known “shuttle-effect” observed in Li-S and Na-S

batteries, where the dissolved polysulfide also migrate to the anode side.<sup>[21]</sup> On the other hand, the formation of the reduced Na-containing products can be highly isolating to create polarization from the anode side, which results in Na degradation during the discharge process.

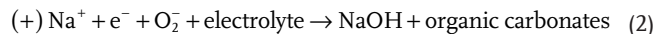
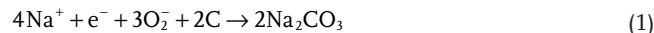
Those results on the Na-O<sub>2</sub> batteries with bare Na are in good agreement with previous reports. Most of the reported Coulombic efficiencies for Na-O<sub>2</sub> batteries in previous literature are much lower than 100%.<sup>[4b,8a,22]</sup> It has been shown that the limited charge efficiency is partially related to the irreversible decomposition of the cell electrolyte, even in the relatively stable ether solvent. By the introduction of the CP on the Na anode, no side product was detected in both XRD pattern and Raman spectrum of the discharged cathode from the Na-O<sub>2</sub> cell in our study (Figure 2b and Figure S4, Supporting Information). Moreover, no obvious evidence of a charging plateau from parasitic reactions was observed, even when the electrode recharged back to 4.5 V. The reappearance of the clean carbon fiber surface further confirms that no discharge product was left on the fully charged cathode (Figure S12, Supporting Information), in agreement with the XRD results for the charged electrode (Figure S5b, Supporting Information). Therefore, it can be concluded based on all the presented evidence that the observed limited Coulombic efficiency can be related to the crossover of O<sub>2</sub><sup>-</sup> from the cathode to anode. In addition, in the case of the cell with bare Na, the side reactions induced by O<sub>2</sub><sup>-</sup> crossover results in the formation of side products, which will gradually cover the Na surface. At the same time, the thick side products on Na surface can block the ion transportation of Na<sup>+</sup> into the electrolyte, and the polarization of the Na-O<sub>2</sub> battery with bare Na increase and trigger the cut-off voltage of the cycling test. The discharge process terminates before the

oxygen diffusion channels were blocked by the discharge products. Therefore, the gradual accumulation of side products on the Na anode is the main reason for the premature ending of the discharge process in Na-O<sub>2</sub> batteries with bare Na anode, leading to a relatively low discharge capacity.

Further comparison of the cells with different separator thicknesses indicates that the discharge capacity of the cell slightly improves by increasing the thickness (Figure S13, Supporting Information), which can be ascribed to the suppression of the side reactions on Na surface caused by O<sub>2</sub><sup>-</sup> crossover. However, this does not mean a thicker separator yields better electrochemical performance. As shown in Figure S13 (Supporting Information), the internal resistance of the cell also increases with increasing separator thickness, leading to a gradual decrease in the cell energy efficiency. At the same time, the achievable charge capacity before voltage drop was slightly increased for both cells compared to the cell with one GF layer, indicating that the short-circuiting issue can only be delayed rather than completely solved by increasing the separator thickness. By comparing the electrochemical performance of the cells with four different configurations, it is easier to find that only the Na-O<sub>2</sub> cell with CP electrically connected with Na metal can effectively prevent the short circuiting issue and exhibit reversible discharge/charge processes at different current densities.

Determining why the CP at the anode side strongly stops the migration of O<sub>2</sub><sup>-</sup> toward the surface of Na anode will be crucial to the future design of battery configurations. We attribute this phenomenon to the different sodium (electro)chemical potential of the CP either self-standing or attached to a Na anode. To determine this difference, we assembled the CP/Na and Na+CP/Na cells and their open circuit potentials are found to be around 1.2 and 0.02 V, respectively. Also, to give a clear picture on the protective effect of CP toward Na anode, the composition of the film-like products on the CP was further characterized by X-ray photoelectron spectroscopy (XPS) and energy dispersive spectroscopy (EDS) techniques. The XPS spectra of C, O, and S elements in both discharged and charged states of CP interlayer are shown in Figure S14 (Supporting Information), and all XPS spectra were calibrated by the standard position of the C–C bond at 284.8 eV. In the C 1s spectrum, the existence of C–O, C=O and COO<sup>-</sup> species on the CP may originate from the decomposition of diethylene glycol dimethyl ether (DEGDME) solvent (Figure S14a,b, Supporting Information).<sup>[23]</sup> Figure S14c,d (Supporting Information) shows the featured peaks of Na<sub>2</sub>CO<sub>3</sub> and NaOH at 531.8 and 532.8 eV, respectively. Meanwhile, the S 2p 3/2 peak at 168.6 eV is likely from the –SO<sub>2</sub><sup>-</sup> fragment after the decomposition of sodium salt (Figure S14e,f, Supporting Information). Therefore, the composition of products on the CP mainly contains NaOH, Na<sub>2</sub>CO<sub>3</sub>, sulfur oxide species, and carboxylic/carbonyl species. More interestingly, no composition difference can be observed at discharge and charge states, which can be further confirmed by the results obtained from EDS line scan on the CP. As shown in Figure S15 (Supporting Information), the Na and O elements follows the same changing trend along the distance, which is different to that of the C element. Also, the ratio of the O to C elements on the CP keeps the same (≈3) at both discharge and charge states. Taking into consideration that

the Na<sub>2</sub>CO<sub>3</sub>, NaOH and other products have formed on CP at the side facing air electrode (Figure S9c, Supporting Information), the following electrochemical reactions are proposed to occur



The attaching of CP onto Na results in a much lower electrochemical potential to provide high potential polarization as the driving force (enhanced kinetics) of the electrochemical reaction based on the Butler–Volmer equation. As a result, these side reactions occur at the CP and produce side products at the CP instead of on the Na surface due to diffusion control, so that less decomposition products will be formed on the Na surface.

Except for the issue of O<sub>2</sub> and O<sub>2</sub><sup>-</sup> crossover, researchers have also verified the generation of reactive species, singlet oxygen (<sup>1</sup>O<sub>2</sub>), in Li- and Na-O<sub>2</sub> batteries recently.<sup>[24]</sup> The <sup>1</sup>O<sub>2</sub> is formed during both discharge and charge process, and charging to higher voltage (>3.3 V) yields significantly more <sup>1</sup>O<sub>2</sub> in the Na-O<sub>2</sub> batteries. More importantly, the authors pointed out that the parasitic chemistry in the Na-O<sub>2</sub> cathode is closely related to the formation of <sup>1</sup>O<sub>2</sub> since the extent of side reactions follows the occurrence of <sup>1</sup>O<sub>2</sub>. Thus, there is no doubt that the <sup>1</sup>O<sub>2</sub> produced during both discharge and charge process also may migrate to the anode side and induce parasitic reactions on the Na surface. Moreover, compared with O<sub>2</sub>, the highly reactive <sup>1</sup>O<sub>2</sub> may induce more serious side reactions.

In the Na-O<sub>2</sub> cells with protected Na, the CP is sandwiched between the Na foil and separator, and thus CP electrically connected with the Na metal to form a protected anode. Actually, the protected Na is equal to a shorted cell, and Na<sup>+</sup> immediately intercalates into the CP and persists in the sodiated state when liquid electrolyte was added. Janek and co-workers have reported that the sodiated CP can react chemically with oxygen to form sodium superoxide.<sup>[9]</sup> Thus, instead of migrating across the CP and trigger electrolyte decomposition on the Na anode, the migrated O<sub>2</sub> from the cathode side during charging (and discharging) will probably react with sodiated carbon (CP) to form NaO<sub>2</sub>, and then electrochemical reactions involving NaO<sub>2</sub> occurs on the CP following the proposed reaction routes in Equations (1)–(3). Therefore, the application of CP on the Na surface not only can alleviate the side reactions induced by O<sub>2</sub><sup>-</sup> crossover, but also somewhat inhibit the detrimental effect of O<sub>2</sub> (and/or <sup>1</sup>O<sub>2</sub>) crossover on the Na anode. As a result, the charge overpotential is significantly reduced and the capacity of the Na-O<sub>2</sub> batteries is boosted due to the reduced accumulation of side product on the Na anode. Instead, the CP merely placed between two GFs may only slightly block the diffusion of O<sub>2</sub><sup>-</sup> by the following chemical reactions





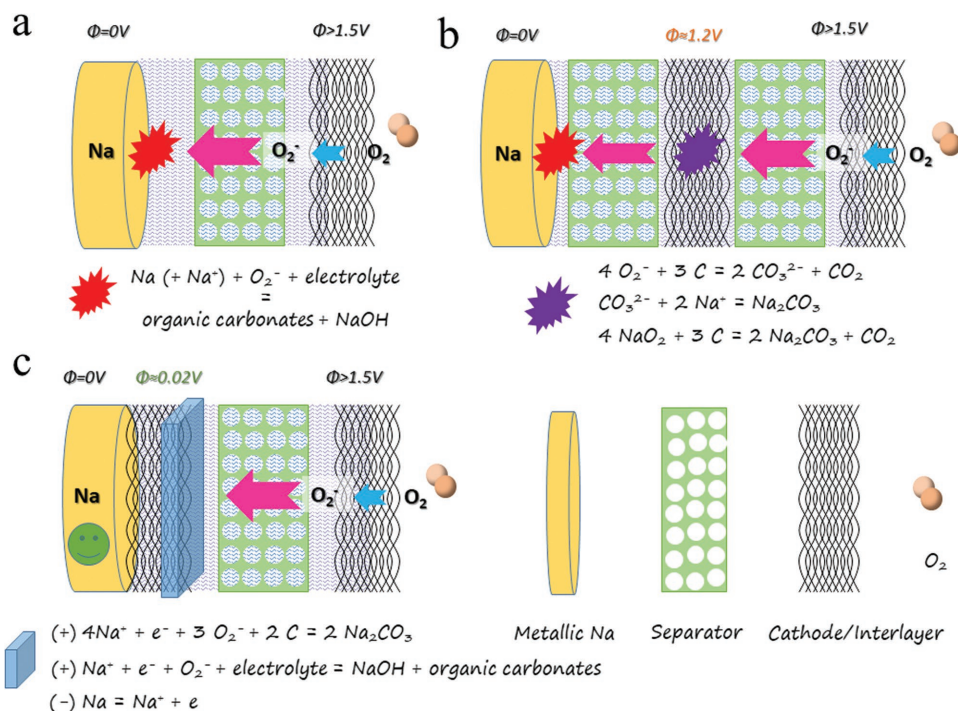


**Figure 6.** Illustration of reaction mechanisms in different Na-O<sub>2</sub> cell configurations. a) The cell with one GF separator, b) the cell with CP sandwiched between two GFs, and c) the cell with CP on the Na anode.

The sluggish rates of the chemical reactions and porous nature of CP make this chemical blocking effect highly inefficient compared to the above electrochemical protection routes. The overall mechanism is depicted in **Figure 6**.

#### 2.4. Discussion on the Dual Critical Roles of CP for Na-O<sub>2</sub> Batteries

A full explanation for the effectiveness of the CP of Na-O<sub>2</sub> batteries can be elucidated in **Figure 7a**. In the Na-O<sub>2</sub> cells with protected Na anode, the function of the CP is beyond that of a simple physical barrier to protect the Na electrode. In the presence of CP, the side reactions involving the O<sub>2</sub> (<sup>1</sup>O<sub>2</sub>) and O<sub>2</sub><sup>-</sup> will preferentially occur on the CP surface by kinetics, which is determined by the cell configuration and the pseudo-equal potential of CP and metallic Na. Thus, the CP acts as a protective layer to alleviate Na degradation during the discharge process and decrease the influence of the metallic Na electrode as a determining factor for the cell discharge capacity. On the other hand, electrons are available on the surface of the conductive CP during Na deposition compared with a nonconductive GF separator. Thus, the CP also plays a role of a 3D current collector, which can decrease the local concentration of current and suppress dendrite growth effectively. Therefore, application of a protected Na with electrically connected Na and CP can thoroughly prevent the short-circuiting issue, while the issue remains when replacing conductive CP with a nonconductive GF.

When the conductive CP is sandwiched between two GFs in the Na-O<sub>2</sub> cell, most O<sub>2</sub> and O<sub>2</sub><sup>-</sup> will still migrate across the CP

and trigger electrolyte decomposition on the Na anode, similar to the case of Na-O<sub>2</sub> cells without a conductive CP on the Na anode (**Figure 7b**). One possible explanation is that a high reduction potential is needed for electrolyte decomposition in the presence of oxidative species (O<sub>2</sub> and O<sub>2</sub><sup>-</sup>). Therefore, the key to the success of this approach is that the conductive CP should be coated directly on the Na metal, making sure that the electrode potential on the CP and metallic Na is the same. This finding is helpful for explaining the fact that the anode experiences more decomposition reactions than the cathode, and the crossover of contaminants from the cathode to the anode makes side reactions more aggravated in Na-O<sub>2</sub> battery system than traditional Na-ion batteries.

The major focus of this study has been the effect of O<sub>2</sub> and O<sub>2</sub><sup>-</sup> crossover toward the metallic Na in Na-O<sub>2</sub> batteries, and emphasizing the important role that the Na anode plays in cell performance. However, the effectiveness of CP in alleviating the side reactions induced by contaminant crossover on the Na anode is not yet totally sufficient. The CP is a porous structure and it cannot fully block the diffusion of O<sub>2</sub> and O<sub>2</sub><sup>-</sup> from the cathode to the Na surface. Therefore, the porous structure of CP still allows a small amount of O<sub>2</sub> and superoxide ions to migrate and reach the Na surface, which also lead to the side reactions. Moreover, conductive CP acts as a sacrificial protective interlayer on the negative electrode, and the conductive surface of the CP will be gradually covered by the side products. Thus, the Na corrosion caused by contaminant crossover can only be alleviated, but not fully eliminated during the long cycling process of cells with CP protected Na. Therefore, effective strategies to restrict the O<sub>2</sub> and O<sub>2</sub><sup>-</sup> crossover toward anode will need to be further developed in the future studies, which

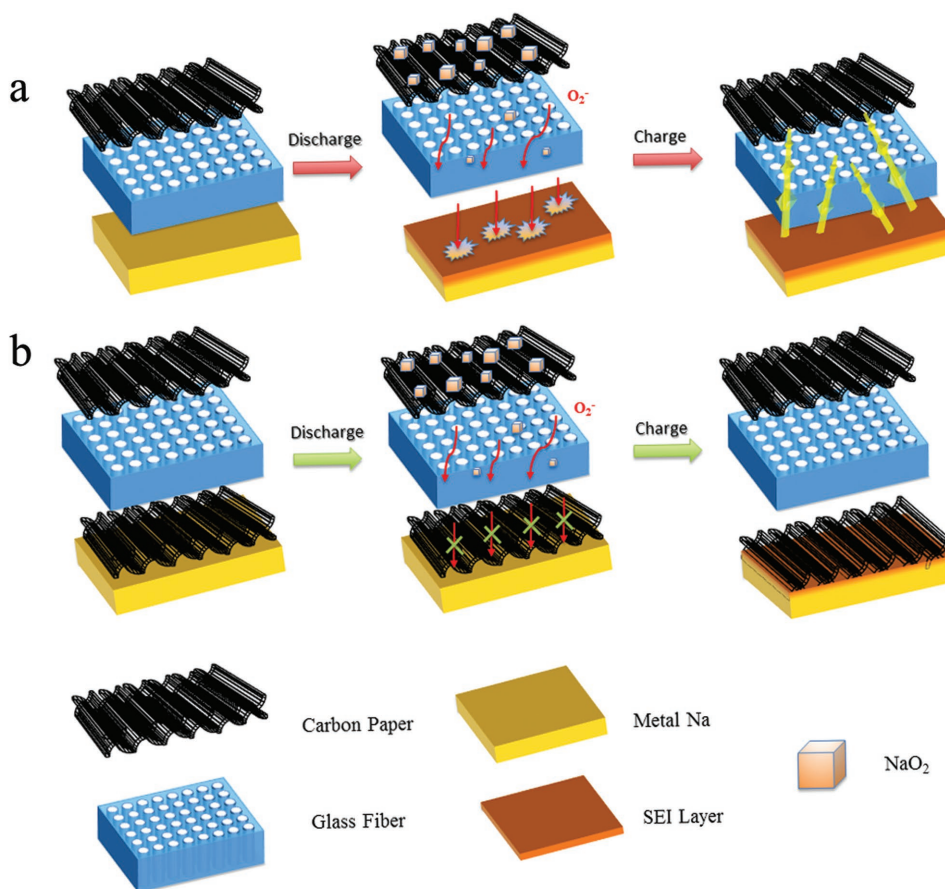


**Figure 7.** Schematic illustration of the discharge and charge process of Na-O<sub>2</sub> batteries with a) bare Na and b) protected Na anode.

will hopefully result in significant improvement in the cycling performance of Na-O<sub>2</sub> batteries.

### 3. Conclusion

In this work, we report a novel design of Na-O<sub>2</sub> battery using electrically connected CP and Na metal as a protected Na anode. The CP demonstrates great effectiveness in addressing the fatal issue of cell short-circuiting by altering the growth and penetration of Na dendrite into dense Na deposition. We show additionally the evidence that the electrolyte decomposition on the Na anode in the presence of O<sub>2</sub> and O<sub>2</sub><sup>-</sup> crossover can be the dominating cause of limited discharge capacity and poor cycling properties of Na-O<sub>2</sub> batteries. The electrochemical potential of the CP gains a pseudo-equal potential when in contact with Na metal, and the side reactions induced by O<sub>2</sub> and O<sub>2</sub><sup>-</sup> crossover preferentially occur on the CP instead of Na surface. The Na corrosion can be alleviated to some extent compared with the cells with bare Na, and a satisfying cycling performance up to 65 cycles with a low charge overpotential can be achieved, which is three times than that of a cell without an interlayer. These results emphasize the important role of Na anode in determining the overall cell performance, and the experience obtained from this work also provides a new avenue for achieving safe and high-performance Na-O<sub>2</sub> batteries and other metal-air batteries.

### 4. Experimental Section

**Materials:** The CP (Freudenberg H23, thickness of 210 μm, porosity of ≈80%), purchased from Fuel Cell Store, was utilized as the cathode and interlayer in the Na-O<sub>2</sub> batteries without further treatment. The surface area of the CP was lower than 1 m<sup>2</sup> g<sup>-1</sup>. DEGDM (reagent grade ≥ 98%, Aldrich) was dried over freshly activated molecular sieves (4 Å, Aldrich) for at least one month before use. Sodium triflate (NaSO<sub>3</sub>CF<sub>3</sub>, Aldrich) was dried under vacuum at 80 °C for 3 d.

**Battery Assembly and Electrochemical Measurements:** The electrochemical performance of Na-O<sub>2</sub> batteries was evaluated with Swagelok-type cells (1/2 in), and the assembly of the cells had been described in detail in the previous work<sup>[6a,25]</sup>; briefly, the Na-O<sub>2</sub> cell using Na foil as the anode, GF as the electrode separator, and CP cathode. The CP and Na metal foil were cut into circular pieces with a geometric surface area of 0.7125 cm<sup>2</sup>. The electrolyte was 0.5 m NaSO<sub>3</sub>CF<sub>3</sub> dissolved in DEGDM, and same amount of electrolyte was applied for comparison in each cell (100 μL). Different from conventional Na-O<sub>2</sub> cells, the Na-O<sub>2</sub> cells with protected Na anode was assembled with CP interlayer sandwiched between Na foil and GF separator, and the cell configuration is shown in Figure S1 (Supporting Information). The electrolyte preparation and battery assembly were carried out in an argon-filled glove box with the oxygen and water contents below 0.1 ppm. The cells were operated under static O<sub>2</sub> with the pressure of 1.5 atm in a homemade testing box, and each cell was stabilized for 20 min at room temperature before electrochemical tests. The galvanostatic discharge-charge tests were carried out using Arbin BT-2000 battery testing system at room temperature. Electrochemical impedance spectroscopy measurements were carried out with a multi potentiostats (VMP3, Biologic).

**Material Characterization:** The morphologies and structures of discharge product were characterized by Hitachi S-4800 field emission SEM, and the morphological studies of the Na anode and separator were performed using a Hitachi 3400N environmental scanning electron microscopy. The Bruker D8 Advance XRD with Cu-K $\alpha$  radiation was used for structural characterization, and the data were collected from 30° to 70° in 2 $\theta$  at a scanning rate of 1° min<sup>-1</sup>. The Raman spectra were collected on a HORIBA Scientific LabRAM Raman spectrometer equipped with a 532.03 nm laser. In this study, the disassembly of the Na-O<sub>2</sub> batteries was carried out in a glove box filled with high-purity Ar. The discharged/charged electrodes and separator were washed by DEGME to remove any residual NaSO<sub>3</sub>CF<sub>3</sub> salt and then rigorously dried in the vacuum chamber before SEM, XRD, and Raman measurements. Leak-tight XRD and Raman sample holders were used to prevent the exposure of air during sample testing. XPS was carried out by a Kratos Axis Ultra Al- $\alpha$  spectrometer operated at 14 kV.

## Supporting Information

Supporting Information is available from the Wiley Online Library or from the author.

## Acknowledgements

X.L. and Q.S. contributed equally to this work. X.L. and Q.S. conceived and designed the experimental work with the help from Y.Z. who proposed method for Na protection; X.L., Q.S., and H.Y. participated in analyzing the experimental results and preparing the manuscript; X.Y. helped with the schematic diagram; C.W. and J.L. performed the XRD characterization; X.L., Q.S., and H.Y. participated in the discussion of the data; X.S. supervised the overall project. All authors have given approval to the final version of the manuscript. This research was supported by National Sciences and Engineering Research Council of Canada, Canada Research Chair Program, Canada Foundation for Innovation, and the University of Western Ontario. X.T. Lin was supported by the Chinese Scholarship Council.

## Conflict of Interest

The authors declare no conflict of interest.

## Keywords

Na anode, Na-O<sub>2</sub> batteries, O<sub>2</sub><sup>-</sup> crossover, side reactions

Received: March 15, 2018

Revised: May 24, 2018

Published online:

- [1] a) F. Cheng, J. Chen, *Chem. Soc. Rev.* **2012**, *41*, 2172; b) P. G. Bruce, S. A. Freunberger, L. J. Hardwick, J.-M. Tarascon, *Nat. Mater.* **2012**, *11*, 19; c) I. Landa-Medrano, C. Li, N. Ortiz-Vitoriano, I. Ruiz de Larramendi, J. Carrasco, T. Rojo, *J. Phys. Chem. Lett.* **2016**, *7*, 1161; d) S. Bing, C. Shuangqiang, L. Hao, W. Guoxiu, *Adv. Funct. Mater.* **2015**, *25*, 4436.
- [2] a) D. Sharon, D. Hirshberg, M. Afri, A. A. Frimer, M. Noked, D. Aurbach, *J. Solid State Electrochem.* **2017**, *21*, 1861; b) D. U. Lee, P. Xu, Z. P. Cano, A. G. Kashkooli, M. G. Park, Z. Chen, *J. Mater. Chem. A* **2016**, *4*, 7107.
- [3] a) B. Sun, X. Huang, S. Chen, P. Munroe, G. Wang, *Nano Lett.* **2014**, *14*, 3145; b) B. Sun, L. Guo, Y. Ju, P. Munroe, E. Wang, Z. Peng, G. Wang, *Nano Energy* **2016**, *28*, 486; c) E. Yoo, H. Zhou, *ACS Nano* **2011**, *5*, 3020.
- [4] a) B. D. McCloskey, J. M. Garcia, A. C. Luntz, *J. Phys. Chem. Lett.* **2014**, *5*, 1230; b) P. Hartmann, C. L. Bender, M. Vračar, A. K. Dürr, A. Garsuch, J. Janek, P. Adelhelm, *Nat. Mater.* **2013**, *12*, 228; c) X. Ren, K. C. Lau, M. Yu, X. Bi, E. Kreydler, L. A. Curtiss, Y. Wu, *ACS Appl. Mater. Interfaces* **2014**, *6*, 19299; d) Y. Zhang, X. Li, M. Zhang, S. Liao, P. Dong, J. Xiao, Y. Zhang, X. Zeng, *Ceram. Int.* **2017**, *43*, 14082.
- [5] a) H. Yadegari, Y. Li, M. N. Banis, X. Li, B. Wang, Q. Sun, R. Li, T.-K. Sham, X. Cui, X. Sun, *Energy Environ. Sci.* **2014**, *7*, 3747; b) C. L. Bender, P. Hartmann, M. Vračar, P. Adelhelm, J. Janek, *Adv. Energy Mater.* **2014**, *4*, 1301863; c) S. Bing, K. Katja, X. Xiuqiang, M. Paul, P. Zhangquan, W. Guoxiu, *Adv. Mater.* **2017**, *29*, 1606816; d) H. Yadegari, C. J. Franko, M. N. Banis, Q. Sun, R. Li, G. R. Goward, X. Sun, *J. Phys. Chem. Lett.* **2017**, *8*, 4794.
- [6] a) Q. Sun, H. Yadegari, M. N. Banis, J. Liu, B. Xiao, X. Li, C. Langford, R. Li, X. Sun, *J. Phys. Chem. C* **2015**, *119*, 13433; b) L. Lutz, D. Alves Dalla Corte, M. Tang, E. Salager, M. Deschamps, A. Grimaud, L. Johnson, P. G. Bruce, J.-M. Tarascon, *Chem. Mater.* **2017**, *29*, 6066; c) C. Xia, R. Black, R. Fernandes, B. Adams, L. F. Nazar, *Nat. Chem.* **2015**, *7*, 496; d) N. Zhao, X. Guo, *J. Phys. Chem. C* **2015**, *119*, 25319; e) Q. Sun, X. Lin, H. Yadegari, W. Xiao, Y. Zhao, K. R. Adair, R. Li, X. Sun, *J. Mater. Chem. A* **2018**, *6*, 1473.
- [7] a) N. Zhao, C. Li, X. Guo, *Phys. Chem. Chem. Phys.* **2014**, *16*, 15646; b) X. Bi, X. Ren, Z. Huang, M. Yu, E. Kreydler, Y. Wu, *Chem. Commun.* **2015**, *51*, 7665; c) L. Medenbach, C. L. Bender, R. Haas, B. Mogwitz, C. Pompe, P. Adelhelm, D. Schröder, J. Janek, *Energy Technol.* **2017**, *5*, 2265.
- [8] a) P. Hartmann, C. L. Bender, J. Sann, A. K. Dürr, M. Jansen, J. Janek, P. Adelhelm, *Phys. Chem. Chem. Phys.* **2013**, *15*, 11661; b) R. Pinedo, D. A. Weber, B. Bergner, D. Schröder, P. Adelhelm, J. Janek, *J. Phys. Chem. C* **2016**, *120*, 8472; c) D. Schröder, C. L. Bender, R. Pinedo, W. Bartuli, M. G. Schwab, Ž. Tomović, J. Janek, *Energy Technol.* **2017**, *5*, 1242.
- [9] C. L. Bender, B. Jache, P. Adelhelm, J. Janek, *J. Mater. Chem. A* **2015**, *3*, 20633.
- [10] H. Yadegari, Q. Sun, X. Sun, *Adv. Mater.* **2016**, *28*, 7065.
- [11] a) C. Xia, R. Fernandes, F. H. Cho, N. Sudhakar, B. Buonacorsi, S. Walker, M. Xu, J. Baugh, L. F. Nazar, *J. Am. Chem. Soc.* **2016**, *138*, 11219; b) T. Liu, G. Kim, M. T. L. Casford, C. P. Grey, *J. Phys. Chem. Lett.* **2016**, *7*, 4841; c) P. Hartmann, M. Heinemann, C. L. Bender, K. Graf, R.-P. Baumann, P. Adelhelm, C. Heiliger, J. Janek, *J. Phys. Chem. C* **2015**, *119*, 22778.
- [12] a) R. S. Assary, J. Lu, P. Du, X. Luo, X. Zhang, Y. Ren, L. A. Curtiss, K. Amine, *ChemSusChem* **2013**, *6*, 51; b) J.-L. Shui, J. S. Okasinski, P. Kenesei, H. A. Dobbs, D. Zhao, J. D. Almer, D.-J. Liu, *Nat. Commun.* **2013**, *4*, 2255; c) B. J. Bergner, M. R. Busche, R. Pinedo, B. B. Berkes, D. Schröder, J. Janek, *ACS Appl. Mater. Interfaces* **2016**, *8*, 7756; d) S. Xin, Y. You, S. Wang, H.-C. Gao, Y.-X. Yin, Y.-G. Guo, *ACS Energy Lett.* **2017**, *2*, 1385.
- [13] a) Q. Sun, H. Yadegari, M. N. Banis, J. Liu, B. Xiao, B. Wang, S. Lawes, X. Li, R. Li, X. Sun, *Nano Energy* **2015**, *12*, 698; b) Q. Sun, J. Liu, X. Li, B. Wang, H. Yadegari, A. Lushington, M. N. Banis, Y. Zhao, W. Xiao, N. Chen, J. Wang, T.-K. Sham, X. Sun, *Adv. Funct. Mater.* **2017**, *27*, 1606662.
- [14] R. Morasch, D. G. Kwabi, M. Tulodziecki, M. Risch, S. Zhang, Y. Shao-Horn, *ACS Appl. Mater. Interfaces* **2017**, *9*, 4374.
- [15] a) G. Q. Zhang, J. P. Zheng, R. Liang, C. Zhang, B. Wang, M. Hendrickson, E. J. Plichta, *J. Electrochem. Soc.* **2010**, *157*,

- A953; b) C. Tran, X.-Q. Yang, D. Qu, *J. Power Sources* **2010**, *195*, 2057.
- [16] a) W. Liu, D. Lin, A. Pei, Y. Cui, *J. Am. Chem. Soc.* **2016**, *138*, 15443; b) W. Luo, Y. Zhang, S. Xu, J. Dai, E. Hitz, Y. Li, C. Yang, C. Chen, B. Liu, L. Hu, *Nano Lett.* **2017**, *17*, 3792; c) D. Lin, J. Zhao, J. Sun, H. Yao, Y. Liu, K. Yan, Y. Cui, *Proc. Natl. Acad. Sci. USA* **2017**, *114*, 4613.
- [17] a) I. Landa-Medrano, R. Pinedo, X. Bi, I. Ruiz de Larramendi, L. Lezama, J. Janek, K. Amine, J. Lu, T. Rojo, *ACS Appl. Mater. Interfaces* **2016**, *8*, 20120; b) L. Lutz, D. A. D. Corte, Y. Chen, D. Batuk, L. R. Johnson, A. Abakumov, L. Yate, E. Azaceta, P. G. Bruce, J.-M. Tarascon, A. Grimaud, *Adv. Energy Mater.* **2018**, *8*, 1701581.
- [18] G. V. Zhuang, H. Yang, B. Blizanac, P. N. Ross, *Electrochem. Solid-State Lett.* **2005**, *8*, A441.
- [19] R. Younesi, M. Hahlin, M. Roberts, K. Edström, *J. Power Sources* **2013**, *225*, 40.
- [20] Z. W. Seh, J. Sun, Y. Sun, Y. Cui, *ACS Cent. Sci.* **2015**, *1*, 449.
- [21] a) M. R. Busche, P. Adelhelm, H. Sommer, H. Schneider, K. Leitner, J. Janek, *J. Power Sources* **2014**, *259*, 289; b) P. G. Bruce, S. A. Freunberger, L. J. Hardwick, J.-M. Tarascon, *Nat. Mater.* **2011**, *11*, 19.
- [22] a) G. A. Elia, I. Hasa, J. Hassoun, *Electrochim. Acta* **2016**, *191*, 516; b) I. Landa-Medrano, R. Pinedo, J. Lu, T. Rojo, *ACS Appl. Mater. Interfaces* **2016**, *8*, 20120; c) F. Wu, Y. Xing, J. Lai, X. Zhang, Y. Ye, J. Qian, L. Li, R. Chen, *Adv. Funct. Mater.* **2017**, *27*, 1700632; d) X. Bi, R. Wang, L. Ma, D. Zhang, K. Amine, J. Lu, *Small Methods* **2017**, *1*, 1700102.
- [23] X. Ren, M. He, N. Xiao, W. D. McCulloch, Y. Wu, *Adv. Energy Mater.* **2017**, *7*, 1601080.
- [24] a) L. Schafzahl, N. Mahne, B. Schafzahl, M. Wilkening, C. Slugovc, S. M. Borisov, S. A. Freunberger, *Angew. Chem., Int. Ed.* **2017**, *56*, 15728; b) N. Mahne, S. E. Renfrew, B. D. McCloskey, S. A. Freunberger, *Angew. Chem., Int. Ed.* **2018**, *57*, 5529.
- [25] H. Yadegari, M. Norouzi Banis, A. Lushington, Q. Sun, R. Li, T.-K. Sham, X. Sun, *Energy Environ. Sci.* **2017**, *10*, 286.